



Control of Coexisting and Chaotic Attractors in Brushless Direct Current Motor

Alex Stephane Kemnang Tsafack^{1,2} · Cyrille Ainamon³ · Andre Cheukem² · Sifeu Takougang Kingni⁴ · Justin Roger Mboupda Pone² · Godpromesse Kenne²

Received: 15 July 2020 / Revised: 31 October 2020 / Accepted: 10 November 2020 / Published online: 3 January 2021
© Brazilian Society for Automatics--SBA 2021

Abstract

Control of coexisting attractors and chaos in brushless direct current motor (BLDCM) is investigated in this paper. Using a weak harmonic modulation of a parameter of the BLDCM, the coexisting attractors between chaotic and period-1-oscillations are destroyed and transformed to period-1-oscillations. Moreover, two single controllers are designed to control the chaotic behavior found in BLDCM. Numerical simulations are used to evaluate the performance of the two developed controllers. Finally, the dynamical behaviors found in BLDCM and the physical feasibility of two proposed single controllers are validated through circuit implementations on OrCAD-PSpice software. The robustness of the three controllers is tested by a sensitivity analysis to parametric uncertainties.

Keywords Brushless direct current motor · Chaotic attractor · Coexisting attractors · Weak harmonic modulation control method · Chaos control · Circuit implementation

1 Introduction

Chaos, hyperchaos, multistability, extreme multistability, antimonotonicity and so on (Pisarchik 2001) have been reported in many fields of engineering including electronic circuits (Linsay 1981), mechanical systems (Thompson and Stewart 2002), biological systems (Hans et al. 2013), electrical machine systems (Cabrera et al. 2015; Bruno et al. 2006; Chau and Wang 2011a; Chen et al. 2001) and so on. Hemati (1994) reported for the first time the chaotic behavior in

BLDCM. BLDCM is the good candidate for manufacturing applications due to their high power density, good speed–torque characteristics, high efficiency, wide speed ranges and low maintenance. BLDCMs have been used in industrial engineering such as linear motors, servomotors, actuators for industrial robots, extruder drive motors and feed drives for DC machine tools (Xia 2012). Computer peripherals (disk drives, printers), handheld power tools (Melkote and Khorrami 1999; Prasetyo et al. 2016) and vehicles ranging from model aircraft to automobiles (Santiago et al. 2012; Hwang et al. 2012; Praveen et al. 2012) are places where you can find BLDCMs.

Unfortunately, chaotic behavior and coexisting attractors in BLDCM are source of instability, unpredictable disturbance (Chau and Wang 2011; Wang et al. 2016). It is therefore important to control chaos behavior and coexisting attractors in this system. Some recent works were focused on controlling chaos used many schemes to achieve the objectives. The global exponential stabilization for the chaotic BLDCM is illustrated in Wan et al. (2014). The sliding mode control scheme of single time-scale BLDCM was investigated in Uyaroğlu and Cevher (2013). Ping et al. 2015 used the stabilization of the fractional-order chaotic BLDCM system via single input; based on the generalized Gronwall inequality, the Mittag–Leffler function was studied. Other

✉ Alex Stephane Kemnang Tsafack
alexstephanekemnang@gmail.com

¹ Research Unit of Condensed Matter of Electronics and Signal Processing, Department of Physics, Faculty of Sciences, University of Dschang, P.O. Box 67, Dschang, Cameroon

² Research Unit of Automation and Applied Computer, Electrical Engineering Department of IUT-FV, University of Dschang, P.O. Box 134, Bandjoun, Cameroon

³ Institut de Mathématiques et de Sciences Physiques, Université D'Abomey-Calavi, B.P. 613, Porto-Novo, Benin

⁴ Department of Mechanical, Petroleum and Gas Engineering, Faculty of Mines and Petroleum Industries, University of Maroua, P.O. Box 46, Maroua, Cameroon

studies of anti-control of chaos in BLDCM are investigated (Ge et al. 2004, 2006a, 2006c). As a result, these control strategies require heavy computational effort and are difficult to implement in real engineering applications.

As far as the authors knowledge, no study on the control of coexisting attractors in BLDCM has been carried out in the literature. So, the objective of this work is twofold: (1) to use a weak harmonic modulation of a parameter of the BLDCM in order to destroy the coexistence between period-1-oscillations and chaotic oscillations and transform BLDCM to period-1-oscillations. (2) To develop two single controllers based on the principle of Lyapunov’s method for asymptotic global stability to control chaos in BLDCM. The single control method is simple, concise and easy to implement. Therefore, the control of coexisting and chaotic attractors in BLDCM is analytically, numerically and electronically analyzed in this paper. The structure of this paper is organized as follows: The control of coexisting attractor in BLDCM using a weak harmonic modulation of a parameter of the BLDCM is performed in Sect. 2. It is followed by the chaos control in BLDCM using single controller in Sect. 3. In Sect. 4, the electronic circuits are implemented to check the existence of chaotic and coexisting attractors found in BLDCM and the effectiveness of the two proposed single controllers. The sensitivity of each control strategy to parametric errors is investigated in Sect. 5. Some concluding remarks are given in Sect. 6.

2 Control of Coexisting Attractors in Brushless Direct Current Motor

The dimensionless form of the mathematical model of the BLDCM without loading conditions is given by Hemati (1994), Ge and Chang (2004), and Ge et al. (2006a, 2006b) as:

$$\frac{dx}{dt} = -x - yz + \rho z, \tag{1a}$$

$$\frac{dy}{dt} = -\delta y + xz, \tag{1b}$$

$$\frac{dz}{dt} = \sigma(x - z) + \eta xy, \tag{1c}$$

where x, y, z denote quadrature–direct-axis current of the motor and angle speed, respectively. The parameters ρ, δ, σ and η are the parameters of BLDCM. For specific value of the parameters σ, η and ρ , system (1) can exhibit chaotic and coexisting attractors as shown in Fig. 1.

System (1) displays double-scroll chaotic attractor in Fig. 1a, while in Fig. 1b, system (1) exhibits double-scroll

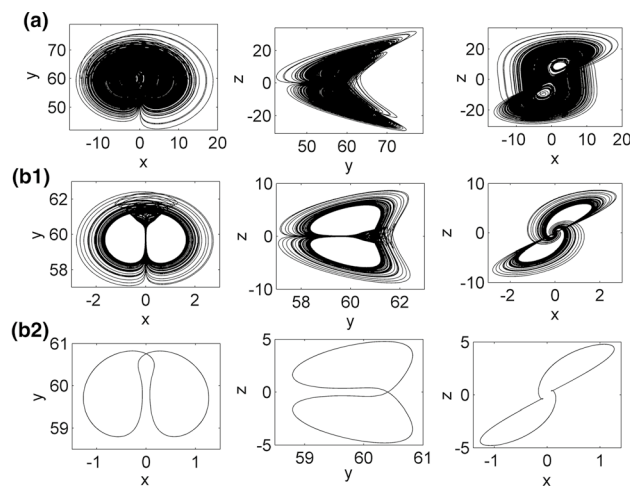


Fig. 1 Phase portraits of chaotic and coexisting attractors for specific value of the parameter δ : **a** $\delta = 0.4$ and **b** $\delta = 0.016$. In panels **a** and **b1**, the initial conditions are $(x(0), y(0), z(0)) = (0.01, 0.01, 0.01)$, while in panel **b2**, the initial conditions are $(x(0), y(0), z(0)) = (1.25, 58.79, 0.0)$. The other parameter values are $\eta = 0.26, \sigma = 4.55$ and $\rho = 60$

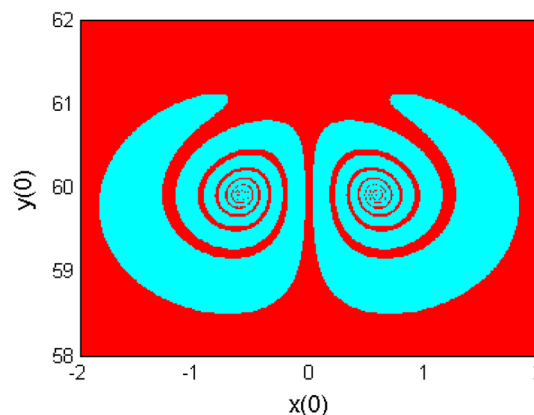


Fig. 2 (Color online) Cross section of the basin of attraction of system (1) in the (x, y) plane at $z = 0$ for $\delta = 0.016, \eta = 0.26, \sigma = 4.55$ and $\rho = 60$

chaotic attractor or periodic attractor as a function of the initial conditions. The basin of attraction of system (1) in the plane $z = 0$ for $\delta = 0.016$ is presented in Fig. 2.

In Fig. 2, the initial conditions in the cyan regions lead to the periodic attractor and those in the red region lead to the chaotic attractor. The control of this phenomenon is discussed by using a weak harmonic modulation control scheme (Pisarchik and Feudel 2014; Ainamon et al. 2019) because of the inconveniences of multistability behavior in many nonlinear systems as well as in BLDCM (Pisarchik 2001; Hemati 1993). Therefore, a weak harmonic modulation is used to replace the parameter δ of system (1) as $\delta = \delta_0 + \delta_c \sin(2\pi f_c t)$ where δ_0 is the initial value of the

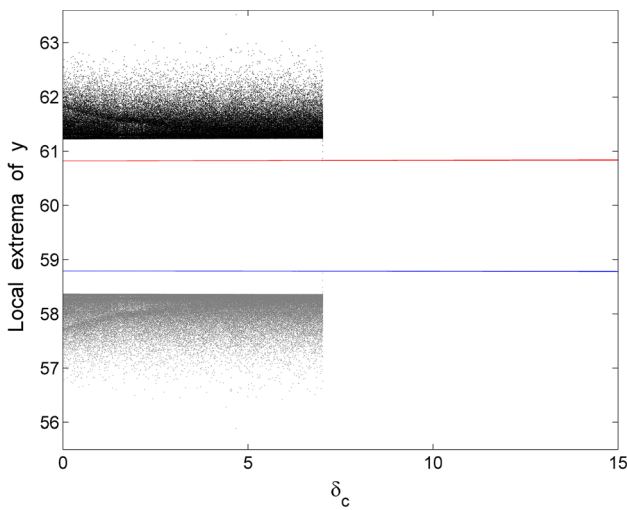


Fig. 3 (Color online) Bifurcation diagram depicting the local extrema of $y(t)$ with respect to the control amplitude parameter δ_c for $\delta_0 = 0.016$, $f_c = 10^{-8}$, $\eta = 0.26$, $\sigma = 4.55$ and $\rho = 60$. The upward (downward) bifurcations are indicated by black (red) dots for local maxima and gray (blue) dot for local minima, respectively

parameter in the uncontrolled system, δ_c and f_c ($f_c \ll f_0 = \sqrt{\delta_0}/2\pi$) are the amplitude and frequency of the control modulation, respectively. The bifurcation diagram depicting the local extrema of variable $y(t)$ versus the control amplitude parameter δ_c is plotted in Fig. 3 in order to check the control of coexisting attractors.

The coexistence between chaotic and periodic attractors is shown in Fig. 3 for $\delta_c \leq 7.02$. While for $\delta_c > 7.02$, this coexistence between chaotic and periodic attractors is converted to periodic attractors. Therefore, the weak harmonic modulation transforms the multistable attractors to monostable one in system (1). The coexisting attractors in system (1) can be clearly see by plotting the phase portraits as shown in Fig. 4 for specific value of control amplitude parameter δ_c .

System (1) displays the coexistence between chaotic oscillations and period-1-oscillations for $\delta_c = 5$ in Fig. 4a. While in Fig. 4b1, b2 where $\delta_c = 14$, the system (1) is actually monostable and the coexisting attractors are converted to period-1-oscillations because of a weak harmonic modulation to parameter δ .

3 Chaos Control of Brushless Direct Current Motor Using Single Controller

A single controller is used in this section to control the chaotic behavior found in BLDCM. Therefore, two simple and single controllers are mathematically designed by using the principle of Lyapunov’s method for asymptotic global stability.

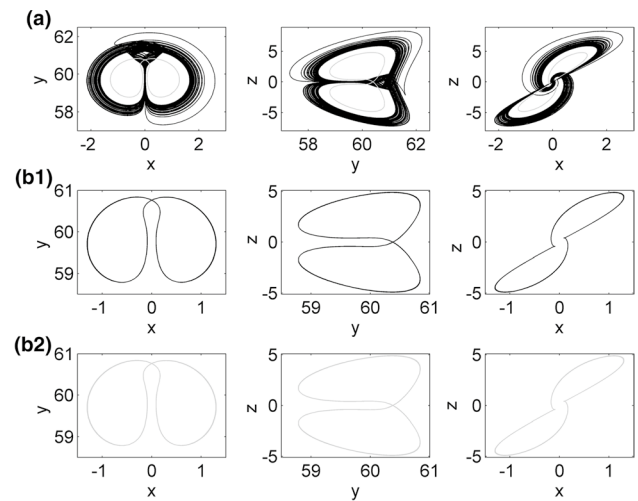


Fig. 4 Phase portraits of system (1) for specific value of control amplitude parameter δ_c : **a** $\delta_c = 5$ and **b** $\delta_c = 14$. The curves in black are obtained using the initial conditions: $(x(0), y(0), z(0)) = (0.01, 0.01, 0.01)$, while the curves in gray are obtained using the initial conditions: $(x(0), y(0), z(0)) = (1.25, 58.79, 0.0)$. The others parameter values are $\delta_0 = 0.016$, $f_c = 10^{-8}$, $\eta = 0.26$, $\sigma = 4.55$ and $\rho = 60$

3.1 Proposed controller 1

In this subsection, the controller u_1 is added to the first equation of system (1):

$$\frac{dx}{dt} = -x - yz + \rho z + u_1, \tag{2a}$$

$$\frac{dy}{dt} = -\delta y + xz, \tag{2b}$$

$$\frac{dz}{dt} = \sigma(x - z) + \eta xy, \tag{2c}$$

where $u_1 = z(y - \rho)$. By substituting the expression of the controller u_1 into the controlled system (2), it becomes:

$$\frac{dx}{dt} = -x, \tag{3a}$$

$$\frac{dy}{dt} = -\delta y + xz, \tag{3b}$$

$$\frac{dz}{dt} = \sigma(x - z) + \eta xy. \tag{3c}$$

The solution of Eq. (3a) is $x(t) = x(0)e^{-t}$. That is yield $\lim_{t \rightarrow \infty} x(t) = 0$. Thus, system (3) can be reduced as follows:

$$\frac{dy}{dt} = -\delta y, \tag{4a}$$

$$\frac{dz}{dt} = -\sigma z, \tag{4b}$$

The solution of system (4) can be rewritten as follows:

$$y(t) = y(0)e^{-\delta t}, \tag{5a}$$

$$z(t) = z(0)e^{-\sigma t}. \tag{5b}$$

That is yield $\lim_{t \rightarrow \infty} y(t) = 0$ and $\lim_{t \rightarrow \infty} z(t) = 0$. Thereafter, the following theorem is given:

Theorem 1 *The chaotic behavior found in the BLDCM can be controlled using the controller $u_1 = z(y - \rho)$.*

Proof The proof is obvious, so leave it out. □

The time series of the state responses and the output of the controller are shown in Fig. 5.

In Fig. 5, the controller u_1 is activated at $t \geq 1400$. It is noted that theorem 1 is effective.

3.2 Proposed controller 2

In this subsection, the controller u_2 is added to the third equation of system (1):

$$\frac{dx}{dt} = -x - yz + \rho z, \tag{6a}$$

$$\frac{dy}{dt} = -\delta y + xz, \tag{6b}$$

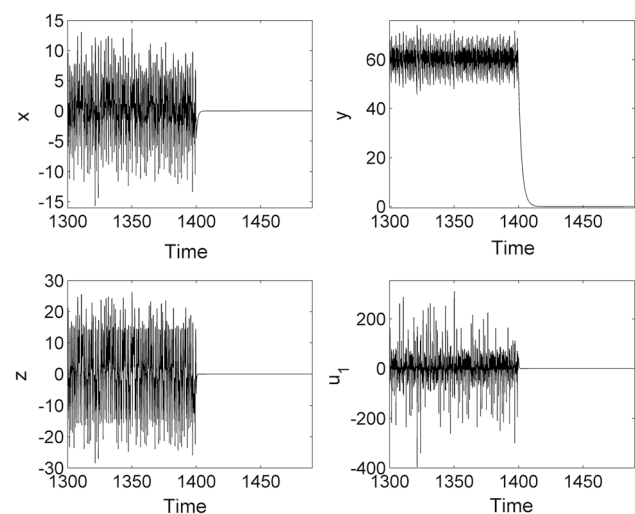


Fig. 5 Time series of x , y , z and the output of the controller u_1 for $\sigma = 4.55$, $\rho = 60$, $\delta = 0.4$ and $\eta = 0.26$. The initial conditions are $(x(0), y(0), z(0)) = (0.01, 0.01, 0.01)$

$$\frac{dz}{dt} = \sigma(x - z) + \eta xy + u_2, \tag{6c}$$

where $u_2 = -x(\eta y + \sigma)$. By substituting the expression of the controller u_2 into the controlled system (6), it becomes:

$$\frac{dx}{dt} = -x - yz + \rho z, \tag{7a}$$

$$\frac{dy}{dt} = -\delta y + xz, \tag{7b}$$

$$\frac{dz}{dt} = -\sigma z. \tag{7c}$$

The solution of Eq. (7c) is $z(t) = z(0)e^{-\sigma t}$. That is yield $\lim_{t \rightarrow \infty} z(t) = 0$. Thus, system (7) can be reduced as follows:

$$\frac{dx}{dt} = -x, \tag{8a}$$

$$\frac{dy}{dt} = -\delta y. \tag{8b}$$

The solution of system (8) is given by:

$$x(t) = x(0)e^{-t}, \tag{9a}$$

$$y(t) = y(0)e^{-\delta t}. \tag{9b}$$

That is yield $\lim_{t \rightarrow \infty} x(t) = 0$ and $\lim_{t \rightarrow \infty} y(t) = 0$. Thereafter, the following theorem is given:

Theorem 2 *The chaotic behavior found in the BLDCM can be controlled using the controller $u_2 = -x(\eta y + \sigma)$.*

Proof The proof is obvious, so leave it out. □

The time series of the state responses and the output of the controller are shown in Fig. 6.

In Fig. 6, the controller u_2 is activated at $t \geq 1400$. It is noted that theorem 2 is effective.

4 Circuit Implementation

The analogue circuitry of system (1) is shown in Fig. 7.

The circuit of Fig. 7 is built by using the operational amplifier working in their linear regime, the ideal multipliers, the resistors and the capacitors. Using the following values of parameters: $C_1 = C_2 = C_3 = 10$ nF, $R_\eta = 384.615$ k Ω (for $\eta = 0.26$), $R_\rho = 1.667$ k Ω (for $\rho = 60$), $R_\sigma = 21.978$ k Ω (for $\sigma = 4.55$), $R_1 = R_2 = R_3 = R_4 = R_5 = R_6 = R_7 = 100$ k Ω the phase portraits of chaotic and coexisting attractors found in

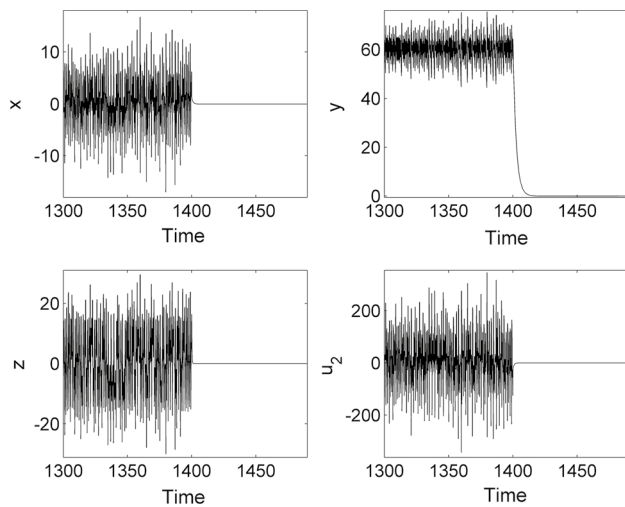


Fig. 6 Time series of x , y , z and the output of the controller u_2 for $\sigma = 4.55$, $\rho = 60$, $\delta = 0.4$ and $\eta = 0.26$. The initial conditions are $(x(0), y(0), z(0)) = (0.01, 0.01, 0.01)$

BLDCM generated from circuit diagram of Fig. 7 are shown in Fig. 8.

The existence of the double-scroll chaotic and coexisting attractors found in BLDCM during the numerical simulations (Fig. 1) can be clearly seen from Fig. 8. The analogue circuitries of the controlled systems (3) and (7) are shown in Fig. 9.

The circuits of Fig. 9 are built by using the operational amplifier working in their linear regime, the ideal multipliers, the resistors, the capacitors and the switches. The switch K of each schematic diagram of the controlled systems (3) and (7) is closed after 1400 ms. The time series of the state responses and the output of the single controller 1 generated from the circuit diagram of Fig. 9a are shown in Fig. 10.

In Fig. 10, the matching of PSpice results with the numerical simulation results of Fig. 5 signifies the feasibility of the proposed single controller 1. The time series of the state responses and the output of the single controller 2 generated from the circuit diagram of Fig. 9b are shown in Fig. 11.

In Fig. 11, the matching of PSpice results with the numerical simulations results of Fig. 6 signifies the feasibility of the proposed single controller 2.

5 Control of Coexisting and Chaotic Attractors in the Presence of Parametric Errors

In this section, the sensitivity of the three proposed controllers to parametric errors is investigated because in real process the parameters used in the control may contain parametric errors (Peruzzi et al. 2016; Balthazar et al. 2012; Avanço et al. 2018). To consider the effects of parametric errors uncertainties on the performance of the three proposed controllers, the parameters used in each control will be considered to have a random error of $\pm 20\%$ (Nozaki et al. 2013; Tusset et al. 2015). Figure 12 presents the controller of coexisting attractors without and with variation in parameters of $\bar{\delta}_c = 14 + 7r(t)$ and $\bar{f}_c = 10^{-8} + 5 \times 10^{-9}r(t)$ where $r(t)$ is the normally distributed random function.

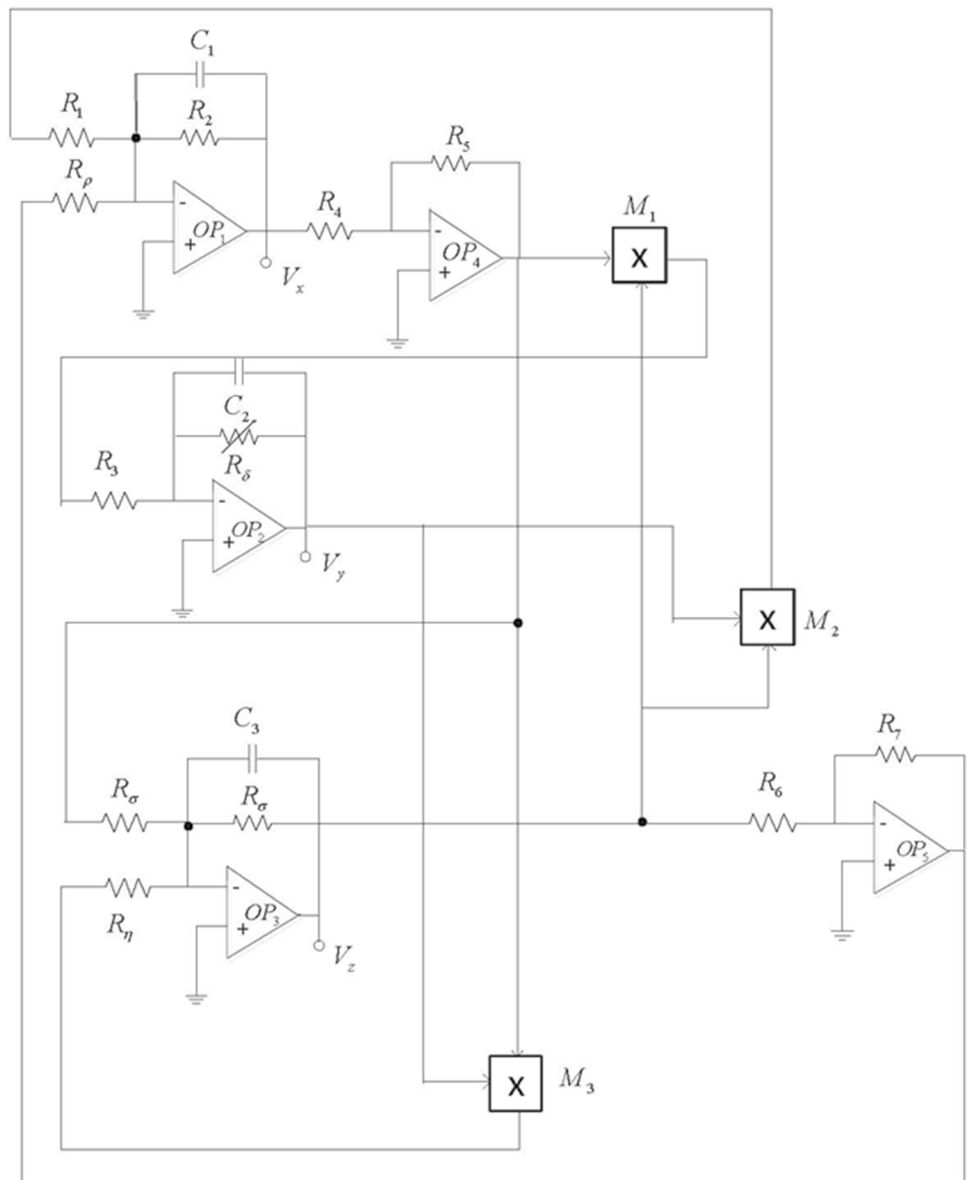
The results of Fig. 12 demonstrate that the controller of coexisting attractors is robust to parametric errors. Figure 13 depicts the two proposed chaos controllers without and with variation in parameters of $\bar{\rho} = 60 + 30r(t)$, $\bar{\eta} = 0.26 + 0.13r(t)$ and $\bar{\sigma} = 4.55 + 2.275r(t)$ where $r(t)$ is the normally distributed random function.

It is clear from Fig. 13 that the two proposed chaos controllers are robust to parametric errors.

6 Conclusion

The development of three controllers to suppress the coexisting attractors and chaos found in brushless direct current motor was performed in this paper. The coexisting of attractors found in brushless direct current motor was controlled to a desired trajectory by using a weak harmonic modulation. Moreover, the two proposed single controllers were designed to suppress the chaotic behavior in brushless direct current motor. In order to access the physical feasibility of the two proposed single controllers and the existence of chaotic and coexisting attractors in brushless direct current motor, electronic circuits were implemented and tested on OrCAD-PSpice software. It was revealed that OrCAD-PSpice validated the numerical simulation results. Thanks to numerical simulations, it was demonstrated that the three proposed controllers are more robust to parametric uncertainties.

Fig. 7 The electronic circuit of the BLDCM described by system (1)



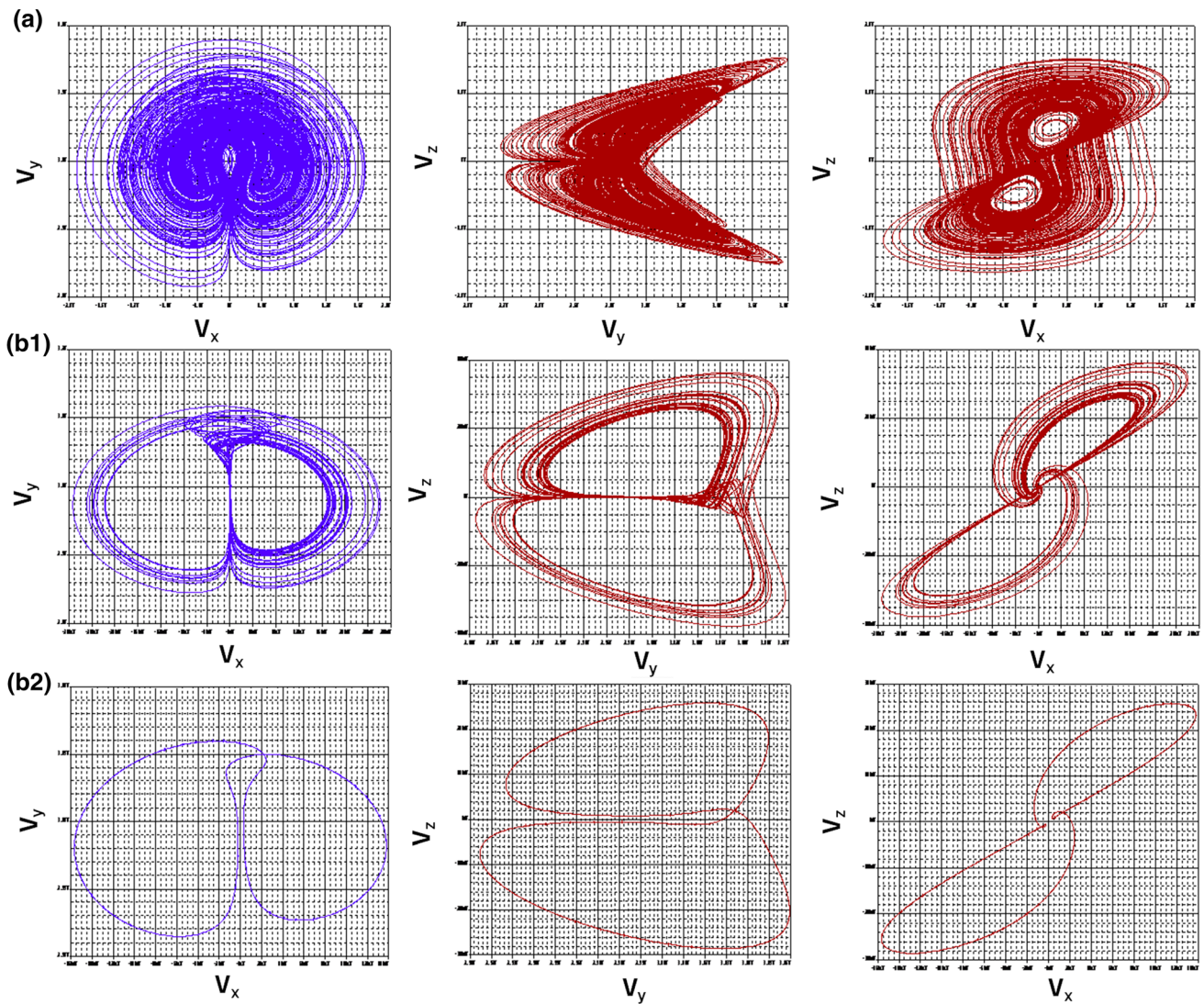


Fig. 8 (Color online) The phase portraits of the chaotic attractor **a** with $R_\eta = 250\text{ k}\Omega$ and coexisting attractors **b** with $R_\eta = 6250\text{ k}\Omega$ in planes (V_x, V_y) , (V_y, V_z) and (V_x, V_z) observed on the PSpice oscil-

loscope. The initial conditions are $V_x(0) = V_y(0) = V_z(0) = 0.01\text{ V}$ in panels **a** and **b1**, while in panel **b2**, the initial conditions are $V_x(0) = 0.0125\text{ V}$, $V_y(0) = 5.879\text{ V}$ and $V_z(0) = 0\text{ V}$

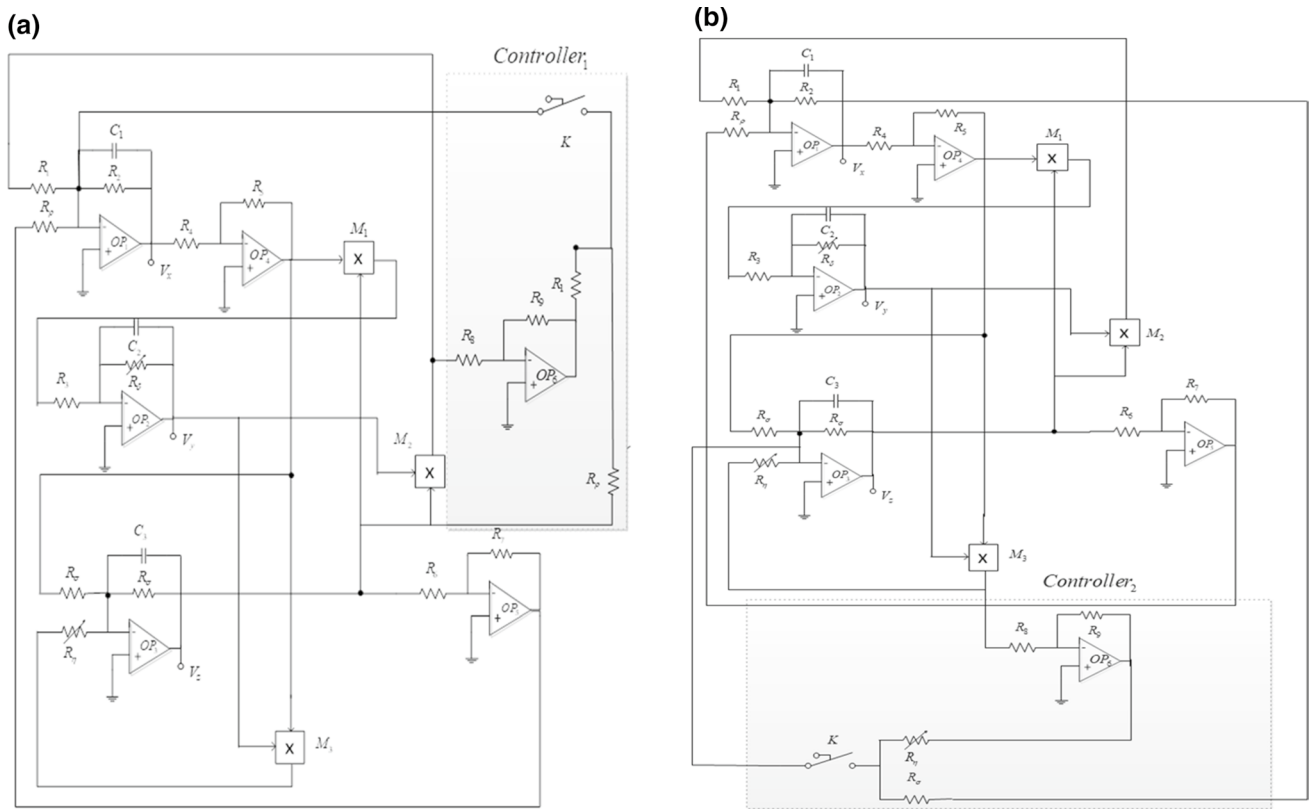


Fig. 9 The electronic circuits of the controlled systems: **a** controlled systems (3) and **b** controlled systems (7)

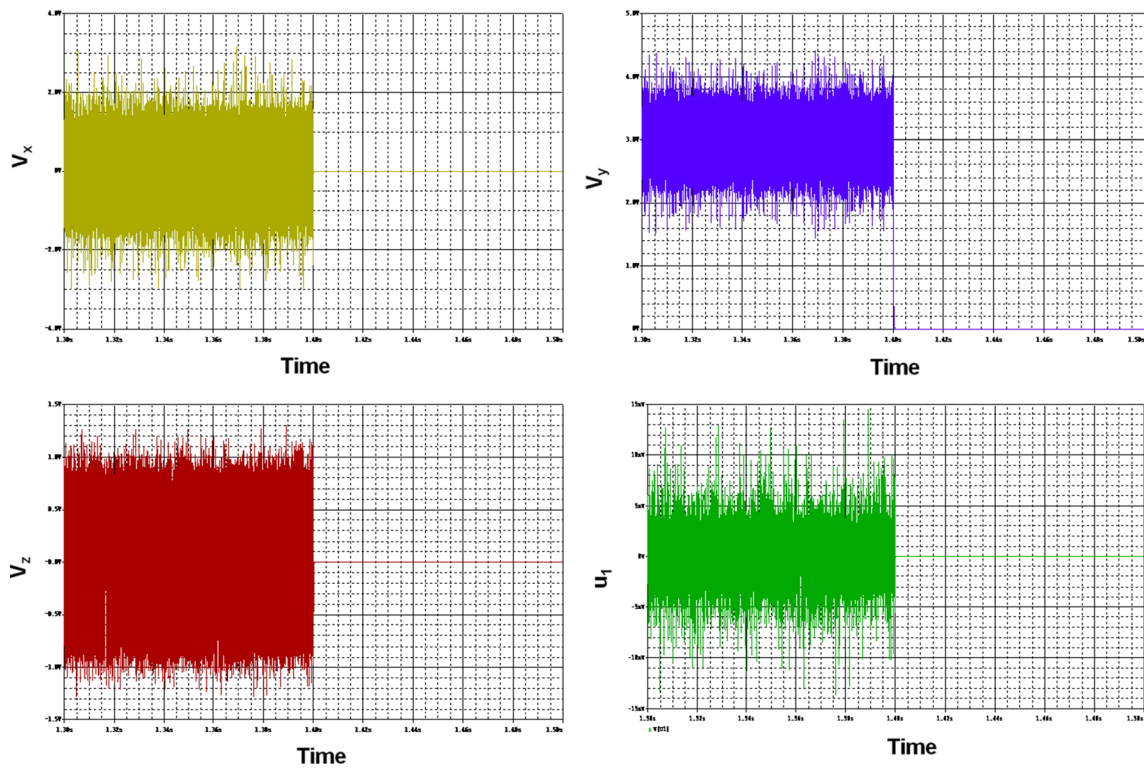


Fig. 10 (Color online) Time series of V_x , V_y , V_z , V_{u_1} of chaos suppression in BLDCM observed on the PSpice oscilloscope

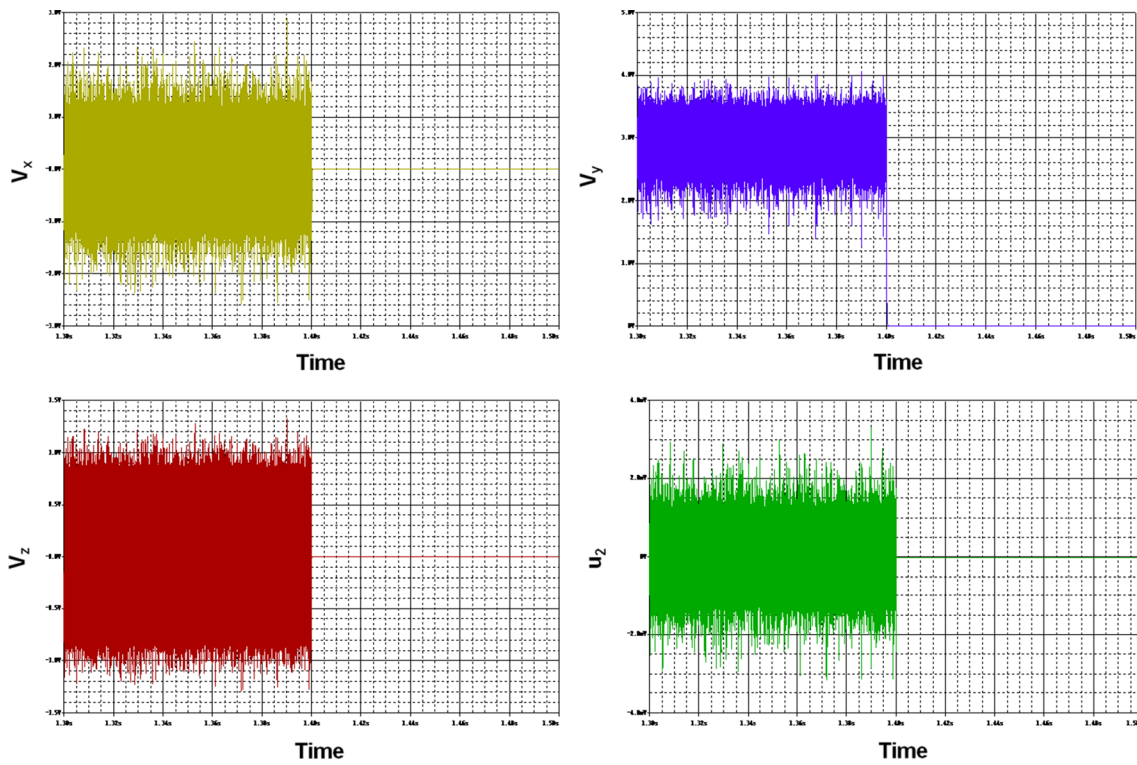


Fig. 11 (Color online) Time series of V_x , V_y , V_z , V_{u_2} of chaos suppression in the BLDCM observed on the PSpice oscilloscope

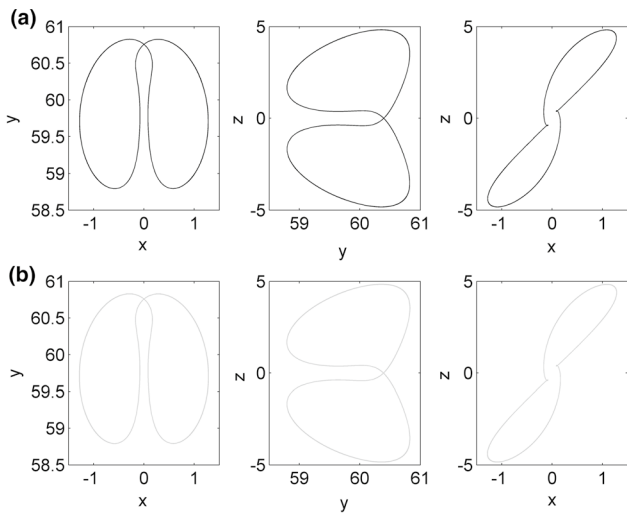


Fig. 12 Coexisting attractors of the BLDCM converted into monostable periodic attractor considering the control without **a** and with **b** uncertainties in parameters: δ_c and f_c . The initial conditions are $(x(0), y(0), z(0)) = (1.25, 58.79, 0.0)$. The other parameter values are $\delta_0 = 0.016, \eta = 0.26, \sigma = 4.55$ and $\rho = 60$

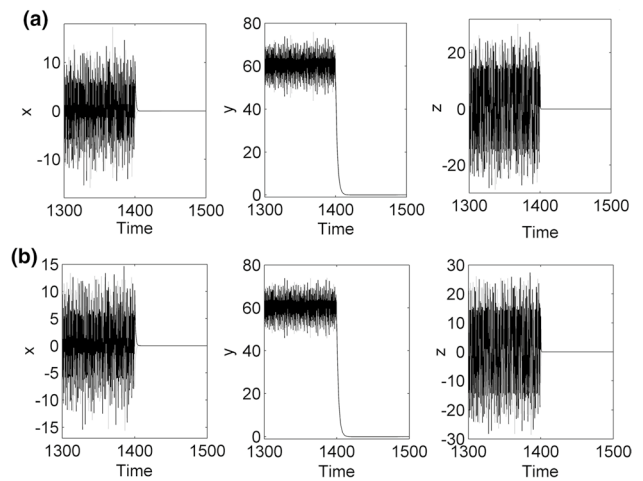


Fig. 13 Time series of x, y, z considering the control without (black lines) and with (gray lines) uncertainties in parameters: **a** ρ (proposed controller 1) and **b** η, σ (proposed controller 2). The initial conditions are $(x(0), y(0), z(0)) = (0.01, 0.01, 0.01)$. The other parameter value is $\delta = 0.4$

References

- Ainamon, C., Kingni, S. T., Tamba, V. K., Chabi Orou, J. B., & Wofo, P. (2019). Dynamics, circuitry implementation and control of an autonomous Helmholtz jerk oscillator. *Journal of Control, Automation and Electrical Systems*, 30, 501–511.
- Avanço, R. H., Tusset, A. M., Balthazar, J. M., Nabarrete, A., & Navarro, H. A. (2018). On nonlinear dynamics behavior of an electro-mechanical pendulum excited by a nonideal motor and a chaos control taking into account parametric errors. *Journal of the Brazilian Society of Mechanical Sciences and Engineering*, 40, 23–39.
- Balthazar, J. M., Tusset, A. M., Souza, S. L. T. D., & Bueno, A. M. (2012). Microcantilever chaotic motion suppression in tapping mode atomic force microscope. *Proceedings of the Institution of Mechanical Engineers Part C Journal of Mechanical Engineering Science*, 227, 1730–1741.
- Bruno, R., Feki, M., & Iu, H. H. C. (2006). Control of a PWM inverter using proportional plus extended time-delayed feedback. *International Journal of Bifurcation and Chaos*, 16, 113–128.
- Cabrera, R. S., Colin, A. H., Roman-Flores, J., & Cabrera, N. S. (2015). Bifurcation analysis of the wound rotor induction motor. *International Journal of Bifurcation and Chaos*, 25, 1550163.
- Chau, K. T., & Wang, Z. (2011a). *Chaos in switched reluctance drive systems* (p. 288). Hoboken: Wiley-IEEE Press.
- Chau, K. T., & Wang, Z. (2011b). *Chaos in electric drive systems: Analysis, control and application*. Singapore: Wiley.
- Chen, J. H., Chau, K. T., & Jiang, Q. (2001). Analysis of chaotic behavior in switched reluctance motors using voltage PWM regulation. *Electric Power Components and Systems*, 29, 211–227.
- Ge, Z. M., & Chang, C. M. (2004). Chaos synchronization and parameters identification of single time scale brushless DC motors. *Chaos, Solitons and Fractals*, 20, 883–903.
- Ge, Z.-M., Chang, C.-M., & Chen, Y.-S. (2006a). Anti-control of chaos of single time-scale brushless DC motor. *Philosophical Transactions of the Royal Society A: Mathematical, Physical and Engineering Sciences*, 364, 2449–2462.
- Ge, Z. M., Chang, C. M., & Chen, Y. S. (2006b). Anti-control of chaos of single time-scale brushless DC motor. *Royal Society of London Transactions Series A*, 364, 2449–2462.
- Ge, Z.-M., Chang, C.-M., & Chen, Y.-S. (2006c). Anti-control of chaos of single time scale brushless dc motors and chaos synchronization of different order systems. *Chaos, Solitons & Fractals*, 27, 1298–1315.
- Ge, Z.-M., Cheng, J.-W., & Chen, Y.-S. (2004). Chaos anticontrol and synchronization of three time scales brushless DC motor system. *Chaos, Solitons & Fractals*, 22, 1165–1182.
- Hans, D., Holden, A. V., & Folke Olsen, L. (Eds.). (2013). *Chaos in biological systems* (Vol. 138). Berlin: Springer.
- Hemati, N. (1993). Dynamic analysis of brushless motors based on compact representations of motion. *Conference Record of the IEEE Industry Applications Society Annual Meeting*, 1, 51–58.
- Hemati, N. (1994). Strange attractors in brushless DC motors. *IEEE Transactions on Circuits and Systems I: Fundamental Theory and Applications*, 41, 40–45.
- Hwang, C. C., Li, P. L., Liu, C. T., & Chen, C. (2012). Design and analysis of a brushless DC motor for applications in robotics. *Electric Power Applications*, 6, 385–389.
- Linsay, P. S. (1981). Period doubling and chaotic behavior in a driven anharmonic oscillator. *Physical Review Letters*, 19(47), 1349–1352.
- Melkote, H., & Khorrami, F. (1999). Nonlinear adaptive control of direct-drive brushless DC motors and applications to robotic manipulators. *IEEE/ASME Transactions on Mechatronics*, 4, 71–81.
- Nozaki, R., Balthazar, J. M., Tusset, A. M., Pontes, B. R., & Bueno, A. M. (2013). Nonlinear control system applied to atomic force microscope including parametric errors. *Journal of Control, Automation and Electrical Systems*, 24, 223–231.
- Peruzzi, N. J., Chavarette, F. R., Balthazar, J. M., Tusset, A. M., Peticarrari, A. L. P. M., & Brasil, R. M. F. L. (2016). The dynamic behavior of a parametrically excited time-periodic MEMS taking into account parametric errors. *Journal of Vibration and Control*, 22, 4101–4110.
- Ping, Z., Bai, R.-J., & Zheng, J.-M. (2015). Stabilization of a fractional-order chaotic brushless DC motor via a single input. *Nonlinear Dynamics*, 82, 519–525.
- Pisarchik, A. N. (2001). Controlling the multistability of nonlinear systems with coexisting attractors. *Physical Review E*, 64, 046203–046207.
- Pisarchik, A. N., & Feudel, U. (2014). Control of multistability. *Physics Reports*, 540, 167–218.
- Prasetyo, H. F., Rohman, A. S., Hariadi, F. I., & Hindersah, H. (2016). Controls of BLDC motor in electric vehicle testing simulator. In *Proceedings of 6th IEEE international conference on system engineering and technology (ICSET)* (pp. 173–178).
- Praveen, R. P., Ravichandran, M. H., Achariand, V. T. S., & Raj, V. P. J. (2012). A novel slot less halfback-array permanent-magnet brushless DC motor for space craft applications. *IEEE Transactions on Industrial Electronics*, 59, 3553–3560.
- Santiago, D., Bernhoff, H., Ekegard, B., Eriksson, S., & Ferhatovic, S. (2012). Electrical motor drivelines in commercial all-electric vehicles: A review. *IEEE Transactions on Vehicular Technology*, 61, 475–484.
- Thompson, J. M. T., & Stewart, H. B. (2002). *Nonlinear dynamics and chaos*. Hoboken: Wiley.
- Tusset, A. M., Piccirillo, V., Bueno, A. M., Balthazar, J. M., Sado, D., Felix, J. L. P., & Brasil, R. M. L. R. D. F. (2015). Chaos control and sensitivity analysis of a double pendulum arm excited by an RLC circuit based nonlinear shaker. *Journal of Vibration and Control*, 22, 3621–3637.
- Uyaroglu, Y., & Cevher, B. (2013). Chaos control of single time-scale brushless DC motor with sliding mode control method. *Turkish Journal of Electrical Engineering & Computer Sciences*, 21, 649–655.
- Wan, L., ShuLuo, X., Zeng, S. Y., & Zhang, B. (2014). Global exponential stabilization for chaotic brushless DC motors with a single input. *Nonlinear Dynamics*, 77, 209–212.
- Wang, L., Fan, J., Wang, Z., Zhan, B., & Li, J. (2016). Dynamic analysis and control of a permanent magnet synchronous motor with external perturbation. *Journal of Dynamic Systems, Measurement, and Control*, 138, 011003–011009.
- Xia, C. (2012). *Permanent magnet brushless DC motor drives and controls*. Singapore: Wiley.

Publisher's Note Springer Nature remains neutral with regard to jurisdictional claims in published maps and institutional affiliations.